A LINEARLY CONFORMING POINT INTERPOLATION METHOD (LC-PIM) FOR PERFECT VISCO-ELASTOPLASTIC ANALYSIS OF 2D SOLIDS

Bui Xuan Thang
Department of Mechanics, Faculty of Mathematics & Computer Science, University of Science, Vietnam National University – HCMC

Nguyen Thoi Trung
Division of Computational Mechanics, Ton Duc Thang University

Nguyen Xuan Hung
Division of Computational Mechanics, Ton Duc Thang University

Phung Van Phuc
Division of Computational Mechanics, Ton Duc Thang University

(Received: 08/05/2013; Revised: 16/08/2013; Accepted: 30/08/2013)

ABSTRACT

A linearly conforming point interpolation method (LC-PIM) was recently proposed for the solid mechanics problems. In this paper, the LC-PIM is further extended to perfect visco-elastoplastic analyses of 2D solids. A dual formulation for the LC-PIM with displacements and stresses as the main variables is performed. The von-Mises yield function and the Prandtl-Reuss flow rule are used. In the numerical procedure, however, the stress variables are eliminated and the problem becomes only displacement-dependent. The numerical results show that the LC-PIM is much more accurate than the FEM and possesses the upper bound property which is very meaningful for the visco-elastoplastic analyses which almost have not got the analytical solutions. This suggests that we can use two models, LC-PIM and FEM, to bound the solution, and can even estimate the global relative error of numerical solutions.

Keywords: Numerical methods, mesh-free methods, linearly conforming point interpolation method (LC-PIM), upper bound, visco-elastoplastic analyses.

Introduction

Many mesh-free methods have been proposed and remarkable progress is achieved in recent years, such as the smooth particle hydrodynamic method [1, 2], general finite difference method [3], the diffuse element method [4], the element-free Galerkin method (EFG) [5], reproducing kernel particle methods [6], the meshless local Petrov–Galerkin method [7], the point interpolation method (PIM) [8–10], etc.

Among the above-mentioned mesh-free methods, PIM is a method based on Galerkin weak form in which the shape functions are constructed using simple interpolation through a set of nodes located in a local support domain. Based on two different basis functions, two types of PIM have been developed including polynomial PIM using polynomial basis functions [8–10] and radial PIM (RPIM) using radial basis functions [11, 12]. Both methods can provide linear consistent shape functions,

however they cannot guarantee a linear exactness of the solutions due to the incompatibility. In two these PIMs, Gauss integration scheme is used to perform the numerical integration.

Recently, a scheme of stabilized conforming nodal integration has been proposed by Chen et al. [13]. In their works, the technique of strain smoothing is introduced in order to eliminate the error in the procedure of direct nodal integration. By using the stabilized conforming nodal integration scheme, the integration constraints can be met and linear exactness in the solution can be guaranteed based on the linear consistent shape functions [13]. Liu *et al.* have applied the scheme of nodal integration into the original PIMs to give the linearly conforming PIM (LC-PIM) for elastic problems [14-16]. The LC-PIM possesses the following novel features: (1) A simple scheme for local supporting node selection is suggested based on triangular or tetrahedral background cells, which overcomes the singular moment matrix issue, and ensures the efficiency in computing PIM shape functions; (2) Shape functions generated using polynomial basis functions and simple interpolation ensure that the PIM shape functions possesses at least linearly consistency and the Delta function property, which facilitates easy implementation of essential boundary conditions; (3) The use of nodal integration scheme with strain smoothing operation converts the domain integration required in the weak form to boundary integrations on the boundary of the smoothing cells, which ensures the conformability of the displacement. Due to these novel features, the LC-PIM is easy to implement, guarantees monotonic convergence, and is computationally efficient.

This paper attempts to further formulate the LC-PIM for perfect visco-elastoplastic analyses of 2D solids. A dual formulation for the LC-PIM with displacements and stresses as the main variables is performed. The von-Mises yield function and the Prandtl-Reuss flow rule are used. In the numerical procedure, however, the stress variables are eliminated and the problem becomes only displacement-dependent. The numerical results show that the LC-PIM is much more accurate than the FEM and possesses the upper bound property which is very meaningful for the visco-elastoplastic analyses which almost have not got the analytical solutions. This suggests that we can use two models, LC-PIM and FEM, to bound the solution, and can even estimate the global relative error of numerical solutions.

Strong formulation for visco-elastoplasticity analyses of 2D solids

In the context of small strain, the total strain $\boldsymbol{\varepsilon}(\mathbf{u}) = \nabla_S \mathbf{u} \in \mathsf{L}^2\left(\Omega; \mathsf{R}^{d\times d}_{\text{sym}}\right)$, where $\nabla_S \mathbf{u}$ denotes the symmetric part of displacement gradient, is separated into two parts

$$\boldsymbol{\varepsilon}(\mathbf{u}) = \mathbf{e}(\boldsymbol{\sigma}) + \mathbf{p}(\xi) \quad (1)$$

where $\xi \in \mathsf{R}^{m\times m}_{\text{sym}}$ is an internal variable, in which $m = 0$ for the case of perfect visco-elastoplasticity, $m = 1$ for the case of the isotropic hardening and $m = d,\ (d = 2,3)$, for the case of the kinematic hardening; $\mathbf{p}(\xi) \in \mathsf{L}^2\left(\Omega; \mathsf{R}^{d\times d}_{\text{sym}}\right)$ is an irreversible plastic strain tensor; and $\mathbf{e}(\boldsymbol{\sigma}) \in \mathsf{L}^2\left(\Omega; \mathsf{R}^{d\times d}_{\text{svm}}\right)$ is elastic strain tensor satisfying $\mathbf{e}(\boldsymbol{\sigma}) = \mathbf{C}^{-1}\boldsymbol{\sigma}$, in which $\mathbf{C}$ is a fourth order tensor of linear isotropic elastic material constants.

To describe properly the evolution process for the plastic strain, it is required to define the admissible stresses, a yield function, and an associated flow rule. In this work, we use the von-Mises yield

function and the Prandtl-Reuss flow rule.

Let $\mathbf{p}$ and Ξ be the kinematic variables of the generalized strain P=(p,ξ), and $\mathbf{\Sigma}=(\boldsymbol{\sigma},\boldsymbol{\alpha})$ be the corresponding generalized stress, where $\boldsymbol{\alpha}\in \mathsf{R}_{\text{sym}}^{m\times m}$ is the hardening parameter describing internal stresses. We define Υ to be the admissible stresses set, which is a closed, convex set, containing $\mathbf{0}$, and defined by

$$\Upsilon=\left\{\Sigma:\Phi(\Sigma)\le 0\right\} \tag{2}$$

where Φ is the von-Mises yield function which is presented specifically for different visco-elastoplastic cases.

In the case of perfect visco-elastoplasticity, the internal stresses ξ and $\boldsymbol{\alpha}$ are omitted, so the von-Mises yield function is

$$\Phi(\boldsymbol{\sigma})=\left\|\text{dev}(\boldsymbol{\sigma})\right\|-\sigma_Y \tag{3}$$

where σ_Y is the yield stress; $\|\mathbf{x}\|$ is the norm of tensor $\mathbf{x}$ and $\text{dev}(\mathbf{x})$ is the deviator tensor of tensor $\mathbf{x}$.

The Prandtl-Reuss flow rule has the form

$$\dot{\mathbf{p}}=\begin{cases}\dfrac{1}{\upsilon}\left(\left\|\text{dev}(\boldsymbol{\sigma})\right\|-\sigma_Y\right) & \text{if } \left\|\text{dev}(\boldsymbol{\sigma})\right\|>\sigma_Y\\ 0 & \text{if } \left\|\text{dev}(\boldsymbol{\sigma})\right\|\le\sigma_Y\end{cases} \tag{4}$$

LC-PIM for visco-elastoplastic analyses of solids: a dual formulation

In the engineering literature, the elastoplastic evolution problem is usually modeled based on the so-called *primal* or *dual* formulation. In the primal formulation [22], the strains are treated as the primary variables and a discretization is required for simultaneous approximations of both the displacement and plastic strain fields. In the dual formulation [22], the displacement and stress approximations are computed simultaneously with *yield functions* and *flow rules* written in terms of *admissible stresses*. In this paper, the dual formulation is used for the LC-PIM.

Galerkin weakform

The visco-elastoplastic problem in Section 2 can now be stated generally in a Galerkin weakform as follows: Seek $\mathbf{u}\in \mathsf{H}^1\left(\Omega;\mathsf{R}^d\right)$ such that $\mathbf{u}=\mathbf{w}_0$ on Γ_D and $\forall\mathbf{v}\in \mathsf{H}_0^1\left(\Omega;\mathsf{R}^d\right)=\left\{\mathbf{v}\in \mathsf{H}^1\left(\Omega;\mathsf{R}^d\right):\mathbf{v}=\mathbf{0}\text{ on }\Gamma_D\right\}$, the following equations are satisfied

$$\int_\Omega \boldsymbol{\sigma}(\mathbf{u}):\boldsymbol{\varepsilon}(\mathbf{v})\mathrm{d}\Omega=\int_\Omega \mathbf{b}\cdot\mathbf{v}d\Omega+\int_{\Gamma_N}\bar{\mathbf{t}}\cdot\mathbf{v}\mathrm{d}\Gamma \tag{5}$$

$$\dot{\mathbf{p}}=\begin{cases}\dfrac{1}{\upsilon}\left(\left\|\text{dev}(\boldsymbol{\sigma})\right\|-\sigma_Y\right) & \text{if } \left\|\text{dev}(\boldsymbol{\sigma})\right\|>\sigma_Y\\ 0 & \text{if } \left\|\text{dev}(\boldsymbol{\sigma})\right\|\le\sigma_Y\end{cases} \tag{6}$$

Time discretization scheme

Equations (5) and (6) are formulated as a sort of time-dependent problem for the "time" $t\in[0,T]$. A generalized midpoint rule [18, 19, 21] is used as the time-discretisation scheme. In each time step, a spatial problem needs to be solved with given variables $(\mathbf{u}(t),\boldsymbol{\sigma}(t),\boldsymbol{\alpha}(t))$ at time t_0 denoted as $(\mathbf{u}_0,\boldsymbol{\sigma}_0,\boldsymbol{\alpha}_0)$ and unknowns at time $t_1=t_0+\Delta t$ denoted as $(\mathbf{u}_1,\boldsymbol{\sigma}_1,\boldsymbol{\alpha}_1)$. Time derivatives are replaced by backward difference quotients; for instance $\dot{\mathbf{u}}$ is replaced by $\dfrac{\mathbf{u}_\vartheta-\mathbf{u}_0}{\vartheta\Delta t}$ where $\mathbf{u}_\vartheta=(1-\vartheta)\mathbf{u}_0+\vartheta\mathbf{u}_1$ with $1/2\le\vartheta\le 1$. The time discrete problem now becomes: Seek $\mathbf{u}_\vartheta\in \mathsf{H}^1\left(\Omega;\mathsf{R}^d\right)$ that satisfied $\mathbf{u}_\vartheta=\mathbf{w}_0$ on Γ_D and

$$\int_\Omega \boldsymbol{\sigma}(\mathbf{u}_\vartheta):\boldsymbol{\varepsilon}(\mathbf{v})\mathrm{d}\Omega=\int_{\Gamma_N}\mathbf{b}_\vartheta\cdot\mathbf{v}\mathrm{d}\Omega+\int\bar{\mathbf{t}}_\vartheta\cdot\mathbf{v}\mathrm{d}\Gamma,\ \forall\mathbf{v}\in \mathsf{H}_0^1\left(\Omega;\mathsf{R}^d\right) \tag{7}$$

$$\frac{1}{\vartheta\Delta t}\begin{bmatrix}\boldsymbol{\varepsilon}(\mathbf{u}_\vartheta-\mathbf{u}_0)-\mathbf{C}^{-1}(\boldsymbol{\sigma}_\vartheta-\boldsymbol{\sigma}_0)\\ \xi(\boldsymbol{\alpha}_\vartheta-\boldsymbol{\alpha}_0)\end{bmatrix}=\frac{1}{\upsilon}\begin{bmatrix}\boldsymbol{\sigma}_\vartheta-\Pi\boldsymbol{\sigma}_\vartheta\\ \boldsymbol{\alpha}_\vartheta-\Pi\boldsymbol{\alpha}_\vartheta\end{bmatrix}\quad\begin{matrix}\text{(a)}\\ \text{(b)}\end{matrix} \tag{8}$$

where $\mathbf{b}_\vartheta = (1-\vartheta)\mathbf{b}_0 + \vartheta\mathbf{b}_1$, $\bar{\mathbf{t}}_\vartheta = (1-\vartheta)\bar{\mathbf{t}}_0 + \vartheta\bar{\mathbf{t}}_1$ in which $\mathbf{b}_0, \bar{\mathbf{t}}_0, \mathbf{b}_1$ and $\bar{\mathbf{t}}_1$ are body forces and surface forces at time t_0, t_1, respectively.

In the plastic phase, it is easy to define $\boldsymbol{\alpha}_\vartheta$ from the Equation (8)(b) [21]. Therefore, the time discretization problem will reduce into solving Equation (7) and Equation (8)(a) which are in fact a dual formulation containing both stress and displacement as field variables [21, 22]. To solve the system of Equations (7) and (8)(a), in this paper, we eliminate one field variable by expressing explicitly the stress $\boldsymbol{\sigma}_\vartheta$ in the form of displacement $\mathbf{u}_\vartheta$ using Equation (8)(a), and then substituting it into Equation (7). The problem will then becomes only displacement-dependent, and we need to solve the resultant form of Equation (7) [21].

Discretization in space by the LC-PIM

In the LC-PIM, the problem domain Ω is discretized into a set of N_n nodes without having the connecting information of elements. However, background cells around nodes are necessary and have to be defined for performing the numerical integration. In the LC-PIM, the background cells are defined based on the Delaunay triangular mesh (for 2D problems) which is generated naturally from the set of N_n field nodes. The following sections will brief the point interpolation and nodal integration scheme with the strain-smoothing operation in the LC-PIM.

Point interpolation in the LC-PIM

In the LC-PIM, polynomials are used to serve as basic functions to create shape functions, and the interpolation is based on a small set of nodes in a local support domain that can overlap with other support domains. Consider a continuous function $u(\mathbf{x})$, which is a displacement component for the visco-elastoplastic problems. It can be approximated in the vicinity of $\mathbf{x}$ as follows

$$u(\mathbf{x}) = \mathbf{p}^T\mathbf{P}_n^{-1}\mathbf{U}_s = \sum_{i=1}^{n}\varphi_i u_i = \Phi^T(\mathbf{x})\mathbf{U}_s \quad (9)$$

where n is the number of polynomial terms, $p_i(\mathbf{x})$ is complete polynomial basis functions and is usually built by utilizing the Pascal's triangles, and $\Phi^T(\mathbf{x})$ is the vector of PIM shape functions,

$$\Phi^T(\mathbf{x}) = \mathbf{p}^T\mathbf{P}_n^{-1} = \{\varphi_1(\mathbf{x}) \quad \varphi_2(\mathbf{x}) \quad \cdots \quad \varphi_n(\mathbf{x})\} \quad (10)$$

The complete polynomial basis of orders 1 and 2 can be written in the following forms

$$\begin{aligned} \mathbf{p}^T(\mathbf{x}) &= \{1 \quad x \quad y\} && \text{Complete 1st order for 2D} \\ \mathbf{p}^T(\mathbf{x}) &= \{1 \quad x \quad y \quad x^2 \quad xy \quad y^2\} && \text{Complete 2nd order for 2D} \end{aligned} \quad (11)$$

The kth derivative of the shape functions can be easily obtained. They are however not required in the LC-PIM due to the use of strain-smoothing operation which will be described in next sub-section.

In the present method, linear monomials are used to serve as the basis functions. This also gives the easiest and also workable way of node selection in which three vertexes of the background three-node triangular cell (for 2D problems) are taken to perform the interpolation of the interest points located inside the cell. This can be easily implemented and can always ensure the invertibility of the moment matrix, as long as the three vertexes of the triangles are not on a line (for 2D problems).

Nodal integration scheme with strain-smoothing operation in the LC-PIM

In the LC-PIM, the background cells are defined based on the Delaunay mesh which is generated naturally from the set of N_n field nodes. In addition, the nodal integration scheme with strain-smoothing operation [13] is adopted to perform the integration. Basing on this Delaunay mesh, the problem domain Ω is divided into N_n background cells Ω_k associated with node *k* such that $\Omega = \bigcup_{k=1}^{N_n} \Omega_k$, in which N_n is the total number of field nodes. For 2D problems, the background cell Ω_k associated with node *k* is generated by sub-triangles of the triangles containing node *k*.

The smoothing domain for each field node is centered by the node and constructed based on the background cells of three-node triangles. As illustrated in Figure 1, the sub-domain of the smoothing domain for node *k* located in the particular cell *j* can be obtained by connecting the mid-edge-points, the centroids of the surface triangles, and the centroid of cell *j*. Finding out other sub-domains located in cells which contain node *k* and the smoothing domain for node *k* can be constructed by uniting all the sub-domains.

In the LC-PIM, the *compatible* total strains $\boldsymbol{\varepsilon} = \nabla_s \mathbf{u}_\vartheta$ in the smoothing domains Ω_k^s associated with node *k* is modified by Chen et al. [17] as follows

$$\bar{\boldsymbol{\varepsilon}}_k = \int_{\Omega_k^s} \boldsymbol{\varepsilon}(\mathbf{x}) \Phi_k(\mathbf{x}) \mathrm{d}\Omega = \int_{\Omega_k^s} \nabla_s \mathbf{u}_\vartheta(\mathbf{x}) \Phi_k(\mathbf{x}) \mathrm{d}\Omega \quad (12)$$

where
$$\Phi_k(\mathbf{x}) = \begin{cases} 1/A_k^s & \mathbf{x} \in \Omega_k^s \\ 0 & \mathbf{x} \notin \Omega_k^s \end{cases} \quad (13)$$

is a smoothing function and A_k^s is the area of the smoothing domain. Substituting Equation (13) into Equation (12) and applying Green formulation, we obtain

$$\bar{\boldsymbol{\varepsilon}}_k = \frac{1}{2A_k^s} \int_{\Gamma_k^s} \mathbf{n}^k \mathbf{u}_\vartheta^T \mathrm{d}\Gamma \quad (14)$$

where Γ_k^s is the boundary of the smoothing domain for node k and $\mathbf{n}^k$ is the outward normal vector matrix of Γ_k^s.

In the discrete version of the problem (7), the spaces $\mathsf{V} = \mathsf{H}^1(\Omega; \mathsf{R}^d)$ and $\mathsf{V}_0 = \mathsf{H}_0^1(\Omega; \mathsf{R}^d)$ are replaced by finite dimensional subspaces $\mathsf{V}^h \subset \mathsf{V}$ and $\mathsf{V}_0^h \subset \mathsf{V}_0$. The discrete problem (7) using the LC-PIM now becomes: Seek $\mathbf{u}_\vartheta \in \mathsf{V}^h$ such that $\mathbf{u}_\vartheta = \mathbf{w}_0$ on Γ_D and

$$\int_\Omega \boldsymbol{\sigma}_\vartheta \left(\bar{\boldsymbol{\varepsilon}}(\mathbf{u}_\vartheta - \mathbf{u}_0) + \mathbf{C}^{-1} \boldsymbol{\sigma}_0 \right) : \bar{\boldsymbol{\varepsilon}}(\mathbf{v}) \mathrm{d}\Omega = \int_\Omega \mathbf{b}_\vartheta \cdot \mathbf{v} \mathrm{d}\Omega + \int_{\Gamma_N} \bar{\mathbf{t}}_\vartheta \cdot \mathbf{v} \mathrm{d}\Gamma \quad \text{for} \quad \forall \mathbf{v} \in \mathsf{V}_0^h \quad (15)$$

Let $(\varphi_1, ..., \varphi_{N_n})$ be the nodal basis of the finite dimensional space V^h, where N_n is the total number of nodes in the problem domain; and φ_i is the independent scalar hat shape function on node satisfying condition Kronecker $\varphi_i(i) = 1$ and $\varphi_i(j) = 0$, $i \neq j$, then the discrete problem now becomes: seeking $\mathbf{u}_\vartheta \in \mathsf{V}^h$ such that $\mathbf{u}_\vartheta = \mathbf{w}_0$ on Γ_D and

$$\mathbf{F}_i = \int_\Omega \boldsymbol{\sigma}_\vartheta \left(\bar{\boldsymbol{\varepsilon}}(\mathbf{u}_\vartheta - \mathbf{u}_0) + \mathbf{C}^{-1} \boldsymbol{\sigma}_0 \right) : \bar{\boldsymbol{\varepsilon}}(\varphi_i) \mathrm{d}\Omega - \int_\Omega \mathbf{b}_\vartheta \cdot \varphi_i \mathrm{d}\Omega - \int_{\Gamma_N} \bar{\mathbf{t}}_\vartheta \cdot \varphi_i \mathrm{d}\Gamma = 0 \quad (16)$$

for $i = 1, ..., N_n$, which produces a set of $N_n d$ nonlinear equations. $\mathbf{F}_i$ in Equation (16) can be written in the form of two parts [21]

$$\mathbf{F}_i(\mathbf{u}_\vartheta) = \mathbf{Q}_i(\mathbf{u}_\vartheta) - \mathbf{P}_i \quad (17)$$

where the part $\mathbf{Q}_i$ depends on $\mathbf{u}_\vartheta$ and is given by

$$\mathbf{Q}_i(\mathbf{u}_\vartheta) \equiv \mathbf{Q}_i = \int_\Omega \boldsymbol{\sigma}_\vartheta \left(\bar{\boldsymbol{\varepsilon}}(\mathbf{u}_\vartheta - \mathbf{u}_0) + \mathbf{C}^{-1} \boldsymbol{\sigma}_0 \right) : \bar{\boldsymbol{\varepsilon}}(\varphi_i) \mathrm{d}\Omega \quad (18)$$

and the part $\mathbf{P}_i$ is independent of $\mathbf{u}_\vartheta$, and is given by

$$\mathbf{P}_i = \int_\Omega \mathbf{b}_\vartheta \cdot \varphi_i \mathrm{d}\Omega + \int_{\Gamma_N} \overline{\mathbf{t}}_\vartheta \cdot \varphi_i \mathrm{d}\Gamma \qquad (19)$$

Iterative solution

In order to solve Equation (16), Newton – Raphson method is used [18, 19, 21]. Moreover, to properly apply the Dirichlet boundary conditions for the nonlinear problem, we use the approach of Lagrange multipliers. Combining the Newton iteration and the set of boundary conditions imposed through Lagrange multipliers $\ddot{\mathbf{e}}$, the extended system of equations is obtained

$$\begin{pmatrix} D\mathbf{F}(\mathbf{u}_\vartheta^p) & \mathbf{G}^T \\ \mathbf{G} & 0 \end{pmatrix} \begin{pmatrix} \mathbf{u}_\vartheta^{p+1} \\ \boldsymbol{\lambda} \end{pmatrix} = \begin{pmatrix} \mathbf{f} \\ \mathbf{w}_0 \end{pmatrix} \qquad (20)$$

with $\mathbf{f} = D\mathbf{F}(\mathbf{u}_\vartheta^p)\mathbf{u}_\vartheta^p - \mathbf{F}(\mathbf{u}_\vartheta^p)$ and $\mathbf{G}$ is a matrix created from Dirichlet boundary conditions such that $\mathbf{G}\mathbf{u}_\vartheta^{p+1} = \mathbf{w}_0$. $D\mathbf{F}$ is in fact the system stiffness matrix whose the local entries are defined as

$$\left(D\mathbf{F}\left(u_{\vartheta,1}^p,...,u_{\vartheta,N_n d}^p\right)\right)_{rw} = \partial \mathbf{F}_r\left(u_{\vartheta,1}^p,...,u_{\vartheta,N_n d}^p\right) \Big/ \partial u_{\vartheta,w}^p \qquad (21)$$

where $r,w \in \Psi_{df}$ which is the set containing degrees of freedom of whole problem domain.

We also note that the trial function $\mathbf{u}_\vartheta(\mathbf{x})$ for elements in the LC-PIM is the same as in the standard FEM and therefore the force vector $\mathbf{P}_i$ in the LC-PIM is computed in the same way as in the FEM.

A-posteriori error estimator

In next section, the numerical performances by the LC-LIM using the complete 1st order polynomial are conducted. The results of LC-PIM will be compared with those of the standard FEM using triangular elements (FEM-T3) [21]. In order to estimate the accuracy of the solution of numerical methods for the visco-elastoplastic problems, a quantitative, fair, and accurate assessment of the numerical solutions is needed. In this assessment for visco-elastoplastic material, we use the following efficient a-posteriori error estimation based on N_e elements Ω_i^e to measure the error in stress solution [18, 19, 21, 23]

$$\eta^h = \frac{\left\|\hat{\boldsymbol{\sigma}}^h - \boldsymbol{\sigma}^h\right\|_{\mathrm{L}^2(\Omega)}}{\left\|\boldsymbol{\sigma}^h\right\|_{\mathrm{L}^2(\Omega)}} = \frac{\left(\sum_{i=1}^{N_e} \int_{\Omega_i^e} \left(\hat{\boldsymbol{\sigma}}^h - \boldsymbol{\sigma}^h\right) : \left(\hat{\boldsymbol{\sigma}}^h - \boldsymbol{\sigma}^h\right) \mathrm{d}\Omega\right)^{1/2}}{\left(\sum_{i=1}^{N_e} \int_{\Omega_i^e} \boldsymbol{\sigma}^h : \boldsymbol{\sigma}^h \mathrm{d}\Omega\right)^{1/2}} \qquad (22)$$

where $\boldsymbol{\sigma}^h$ is the numerical stress in an element by the numerical methods. For the FEM, the element stress is computed directly, while for the LC-PIM models, the element stress is computed by (area-weighted) averaging of stresses of smoothing domains associated with that element [18, 19-23]; and $\hat{\boldsymbol{\sigma}}^h$ is the recovery stress in an element defined by

$$\hat{\boldsymbol{\sigma}}^h = \sum_{j=1}^{3} N_j(\mathbf{x}) \boldsymbol{\sigma}^h(\mathbf{x}_j) \qquad (23)$$

where $N_j(\mathbf{x})$ are the linear shape functions of triangles used in the standard FEM, and $\boldsymbol{\sigma}^h(\mathbf{x}_j)$ are stress values at node $\mathbf{x}_j$ of the element of any numerical methods. For the LC-PIM, the stress $\boldsymbol{\sigma}^h(\mathbf{x}_j)$ at node $\mathbf{x}_j$ is computed directly, while for the FEM-T3,

$\boldsymbol{\sigma}^h(\mathbf{x}_j)$ is computed by (area-weighted) averaging of stresses of elements or of smoothing domains surrounding node $\mathbf{x}_j$ [18, 19-23].

The quantity η^h can monitor the local spatial approximation error, and a larger value of η^h implies a larger spatial error. Also note that in the case the problem has the analytical solution, the recovery stress $\hat{\boldsymbol{\sigma}}^h$ is replaced by the exact stress σ, and the estimated error η^h will become the exact error η.

A numerical example

In this section, the properties of LC-PIM are observed through a numerical example computed for perfect visco-elastoplasticity. The example is for the 2D problems and the numerical results of LC-PIM will be compared with those of FEM-T3 [21].

2D plate with a circular hole: perfect visco-elastoplasticity

Figure 3 represents a 2D plate $\Omega = [-2,2]\times[-2,2]$ with a central circular hole, radius $a = 1m$, subjected to time dependent surface forces $g(t) = 500t$ at the top and the bottom edges. The rest of the boundary is free. There is no volume force.

Because of the axis-symmetric characteristic of the problem, only the upper right quadrant of the plate is modeled as shown in Figure 3, and symmetric conditions are imposed on the left and bottom edges, and the inner boundary of the hole is traction free. Figure 4 gives a discretization of the domain using 81 nodes for a quarter of plate. Assuming that the material is perfect visco-elastoplasticity with Young's modulus $E = 206,900$, Poisson's ratio $\upsilon = 0.29$, yield stress $\sigma_Y = 450$, and the initial data for the stress vector σ_0 is set zero.

The solution is computed in the time interval from $t = 0.03$ to $t = 0.3$ in 10 uniform steps of time $\Delta t = 0.03$. Using the mesh as shown in Figure 4, the material remains elastic (iteration = 1) in six first steps between $t = 0.03$ and $t = 0.18$ for all -two numerical methods as shown in Table 1. The material becomes plastic at $t = 0.21$ (iteration > 1). The number of iterations in Newton's method of LC-PIM and FEM-T3 also shown in Table 1 is almost the same, but the estimated errors η^h by Equation (22) of LC-PIM are about two times less than those of FEM-T3.

Figure 5 shows the evolution process of the elastic shear energy density $\left\|\text{dev}(\hat{\boldsymbol{\sigma}}^h)\right\|^2/(4\mu)$ at four different time instances by using the LC-PIM. It is seen that the plasticity domain first appears at the corner containing point $A(1,0)$ and then at the corner containing point $B(0,1)$.

The comparison between the displacements of points $A(1,0)$ and those of point $B(0,1)$ at different time steps is shown in Table 2. The results show that the displacements of LC-PIM are larger than those of FEM-T3. This implies that the LC-PIM is softer than the FEM-T3. This property can be illustrated even clearer in Figure 6 which shows the convergence of the elastic strain energy $E = \int_\Omega \boldsymbol{\sigma}_\vartheta : \mathbf{e}_\vartheta d\Omega$ versus the degrees of freedom at $t = 0.2$. The results show clearly that the LC-PIM is soft and gives an upper bound of the exact solution while the FEM-T3 is stiff and gives a lower bound.

This upper bound property of LC-PIM is very meaningful in these visco-elastoplasticity analyses which almost have not got the analytical solutions. This suggests that we can use two models, LC-PIM and FEM-T3 (or other finite element methods that give the lower bound), using only the displacement at nodes as the field variables to bound the solution. For example, Table 3 shows the global relative error e (%) in the elastic strain energy $E = \int_\Omega \boldsymbol{\sigma}_\vartheta : \mathbf{e}_\vartheta d\Omega$ between the

solution of LC-PIM and that of FEM-T3 at $t = 0.3$. In this case, we even do not need the exact solution to evaluate the error *e*. It is seen that the error *e* decreases from 5.18% to 0.32% when the degrees of freedom (DOFs) increase from 182 to 3306. These results illustrate clearly a relative evaluation about the accuracy of numerical solutions.

Conclusion

This paper attempts to further formulate the LC-PIM for more complicated visco-elastoplastic analyses of 2D using Delaunay triangular meshes. The material behavior includes perfect visco-elastoplasticity. A dual formulation for the LC-PIM with displacements and stresses as the main variables is performed. The von-Mises yield function and the Prandtl-Reuss flow rule are used. In the numerical procedure, however, the stress variables are eliminated and the problem becomes only displacement-dependent. The numerical results of LC-PIM in comparison with those of FEM-T3 lead to the following remarks:

- The LC-PIM is soft and gives an upper bound (in displacement and elastic strain energy) of the exact solution while the FEM-T3 is stiff and gives lower bounds. This suggests that we can use two models, LC-PIM and FEM-T3 using triangular elements to bound the solution: in both displacement and stress solutions. The reliability of numerical results is hence increased significantly. We can even estimate the global relative error of numerical solutions without knowing the exact solution. In particular, these models use only the displacement at nodes as the field variables and their numerical performance is quite straightforward.
- The a-posteriori estimated error η^h used in this work is shown to be reliable in estimating the error of the stress solution of all numerical methods used. For 2D problems, the a-posteriori estimated error η^h of the LC-PIM is about 2-3 times smaller than those of FEM-T3.

Acknowledgement

The authors are thankful to the University of Science of Hochiminh City, Vietnam, for supporting the necessary financial assistance for carrying out the present research.

REFERENCES

[1] Lucy LB. A numerical approach to testing the fission hypothesis. The Astronomical Journal 1977; 8(12):1013–1024.

[2] Liu GR, Liu MB. Smoothed Particle Hydrodynamics—A Meshfree Practical Method. World Scientific: Singapore, 2003.

[3] Liszka T, Orkisz J. The finite difference methods at arbitrary irregular grids and its applications in applied mechanics. Computers and Structures 1980; 11:83–95.

[4] Nayroles B, Touzot G, Villon P. Generalizing the finite element method: diffuse approximation and diffuse elements. Computational Mechanics 1992; 10:307–318.

[5] Belytschko Y, Lu YY, Gu L. Element-free Galerkin methods. International Journal for Numerical Methods in Engineering 1994; 37:229–256.

[6] Liu WK, Jun S, Zhang YF. Reproducing kernel particle methods. International

Journal for Numerical Methods in Engineering 1995; 20:1081–1106.

[7] Atluri SN, Zhu T. A new meshless local Petrov–Galerkin (MLPG) approach in computational mechanics. Computational Mechanics 1998; 22:117–127.

[8] Liu GR, Gu YT. A point interpolation method for two-dimensional solids. International Journal for Numerical Methods in Engineering 2001; 50:937–951.

[9] Liu GR. Meshfree Methods: Moving Beyond the Finite Element Method. CRC Press: Boca Raton, FL, 2002.

[10] Liu GR, Gu YT. An Introduction to Meshfree Methods and their Programming. Springer: Dordrecht, The Netherlands, 2005.

[11] Wang JG, Liu GR. A point interpolation meshless method based on radial basis functions. International Journal for Numerical Methods in Engineering 2002; 54:1623–1648.

[12] Liu GR, Zhang GY, Gu YT, Wang YY. A meshfree radial point interpolation method (RPIM) for three-dimensional solids. Computational Mechanics 2005; 36(6):421–430.

[13] Chen JS, Wu CT, Yoon S, You Y. A stabilized conforming nodal integration for Galerkin mesh-free methods. International Journal for Numerical Methods in Engineering 2001; 50:435–466.

[14] Liu GR, Zhang GY, Dai KY, Wang YY, Zhong ZH, Li GY, Han X. A linearly conforming point interpolation method (LC-PIM) for 2D solid mechanics problems. International Journal of Computational Methods 2005; 2(4):645–665.

[15] Liu GR, Li Y, Dai KY, Luan MT, Xue W. A linearly conforming RPIM for 2D solid mechanics. International Journal of Computational Methods 2006.

[16] Zhang GY, Liu GR, Wang YY, Huang HT, Zhong ZH, Li GY, Han X. A linearly conforming point interpolation method (LC-PIM) for three-dimensional elasticity problems. International Journal for Numerical Methods in Engineering 2007; 72:1524–1543.

[17] J.S. Chen, C.T. Wu, S. Yoon, Y. You, A stabilized conforming nodal integration for Galerkin meshfree method, International Journal for Numerical Methods in Engineering. 50 (2001) 435-466.

[18] T. Nguyen-Thoi, G.R. Liu, H.C. Vu-Do, H. Nguyen-Xuan, An edge-based smoothed finite element method (ES-FEM) for visco-elastoplastic analyses in 2D solids using triangular mesh, Computational Mechanics. 45 (2009) 23-44.

[19] T. Nguyen-Thoi**,** G.R. Liu, H.C. Vu-Do, H. Nguyen-Xuan, A face-based smoothed finite element method (FS-FEM) for visco-elastoplastic analyses of 3D solids using tetrahedral mesh, Computer Methods in Applied Mechanics and Engineering. 198 (2009) 3479-3498.

[20] G.R. Liu, T. Nguyen-Thoi, K.Y. Lam, A novel Alpha Finite Element Method (αFEM) for exact solution to mechanics problems using triangular and tetrahedral elements, Computer Methods in Applied Mechanics and Engineering. 197 (2008) 3883-3897.

[21] C. Carstensen, R. Klose, Elastoviscoplastic Finite Element Analysis in 100 lines of Matlab, Journal of Numerical Mathematics. 10 (2002) 157-192.

[22] W. Han, B.D. Reddy, Computational plasticity: The variational basis and numerical

analysis, Computational Mechanics Advances. 2 (1995) 283:400.

[23] C. Carstensen, S.A. Funken, Averaging technique for FE-a posteriori error control in elasticity. Part 1: Conforming FEM, Computer Methods in Applied Mechanics and Engineering. 190 (2001) 2483-2498.

[24] G.L. Liu, Nguyen Thoi Trung, Smoothed Finite Element Methods. CRC Press: Boca Raton, Florida, 2010.

TABLES

Table 1. Number of iterations and the estimated error η^h using the FEM-T3 and LC-PIM at various time steps for the 2D plate with hole

Step	FEM-T3		LC-PIM	
	Iterations	η^h	Iterations	η^h
t=0.03	1	0.0792	1	0.0357
t=0.06	1	0.0792	1	0.0357
t=0.09	1	0.0792	1	0.0357
t=0.12	1	0.0792	1	0.0357
t=0.15	1	0.0792	1	0.0357
t=0.18	1	0.0792	1	0.0357
t=0.21	3	0.0792	1	0.0357
t=0.24	4	0.0816	3	0.0357
t=0.27	4	0.0874	3	0.0329
t=0.30	4	0.0933	4	0.0327

Table 2. Horizontal displacement u_A at point A(1,0) and vertical displacement v_B at point B(0,1) using FEM-T3 and LC-PIM at various time steps for the 2D plate with hole

Step	FEM-T3		LC-PIM	
	u_A	v_B	u_A	v_B
t=0.03	-0.312	0.4862	-0.321	0.4978
t=0.06	-0.624	0.9724	-0.642	0.9956
t=0.09	-0.936	1.4586	-0.963	1.4934
t=0.12	-1.248	1.9448	-1.284	1.9911
t=0.15	-1.56	2.4311	-1.6051	2.4889
t=0.18	-1.871	2.9173	-1.9261	2.9867
t=0.21	-2.184	3.4038	-2.2466	3.4852
t=0.24	-2.503	3.9016	-2.5688	4.0002
t=0.27	-2.823	4.4286	-2.8973	4.5524
t=0.30	-3.159	4.9956	-3.218	5.152

Table 3. Global relative error e (%) in the elastic strain energy $E = \int_{\Omega} \boldsymbol{\sigma}_{\vartheta} : \mathbf{e}_{\vartheta} d\Omega$ at $t = 0.3$ between the solution of FEM-T3 and that of LC-PIM for the 2D plate with hole

DOFs	Elastic strain energy E_1 by FEM-T3	Elastic strain energy E_2 by LC-PIM	Global relative error (%) $e = \frac{\lvert E_1 - E_2 \rvert}{E_1 + E_2} \times 100\%$
182	0.2803	0.3109	5.18
256	0.2871	0.3057	3.14
462	0.2907	0.3032	2.10
650	0.2929	0.3018	1.50
870	0.2942	0.3010	1.14
1122	0.2951	0.3004	0.89
1406	0.2958	0.3000	0.70
1722	0.2963	0.2997	0.57
2450	0.2969	0.2994	0.42
3306	0.2973	0.2992	0.32

FIGURES

Figure 1. Example of triangle background cells and the supporting node domains

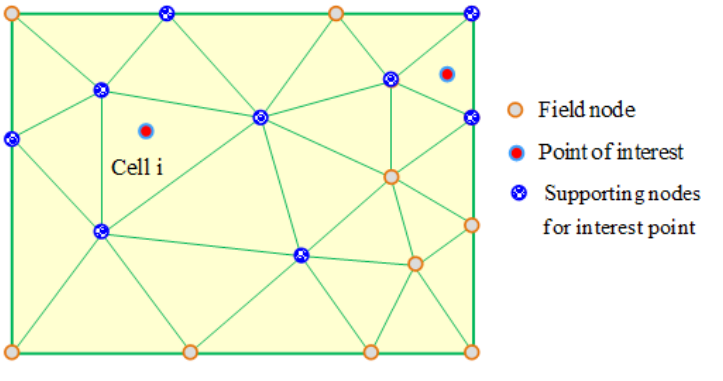

Figure 2. Background cells are based on the Delaunay triangular mesh and the smoothing domains are associated with nodes in the LC-PIM

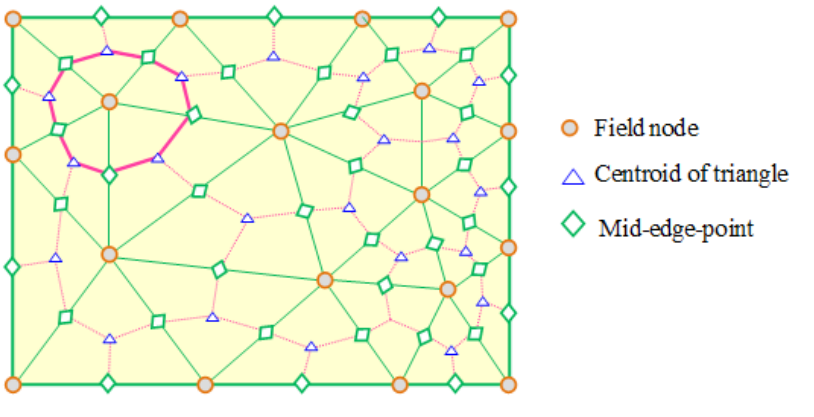

Figure 3. Plate with a circular hole subjected to time dependent surface forces *g(t)* and its quarter model with symmetric conditions imposed on the left and bottom edges

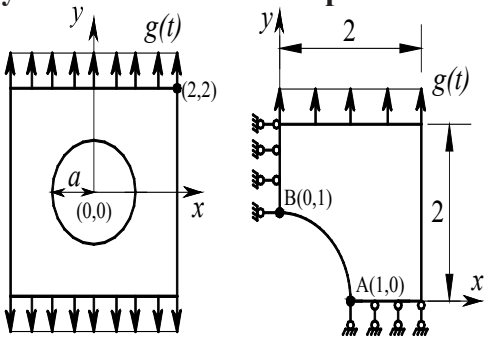

Figure 4. A domain discretization using 81 nodes for a quarter of plate with a circular hole subjected to time dependent surface forces *g(t)*

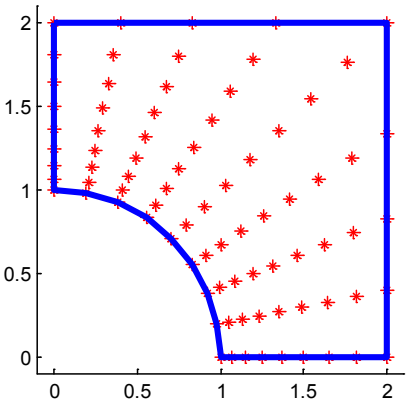

Figure 5. Evolution of the elastic shear energy density $\left\|\mathrm{dev}(\hat{\boldsymbol{\sigma}}^h)\right\|^2/(4\mu)$ using the LC-PIM at some different time steps for the axis-symmetric ring problem; a) t = 0.1; b) t = 0.15; c) t = 0.2; d) t = 0.25

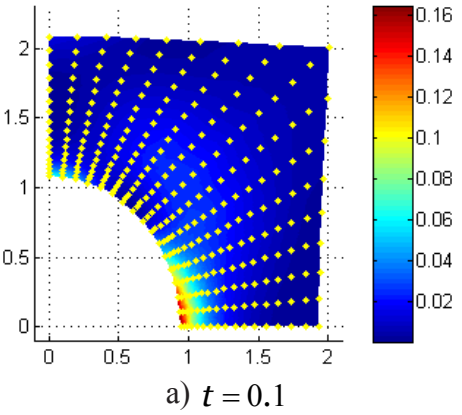

a) $t = 0.1$

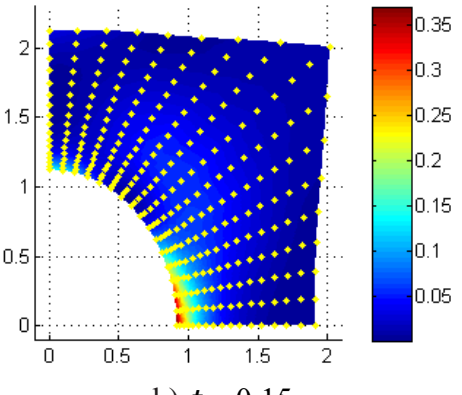

b) $t = 0.15$

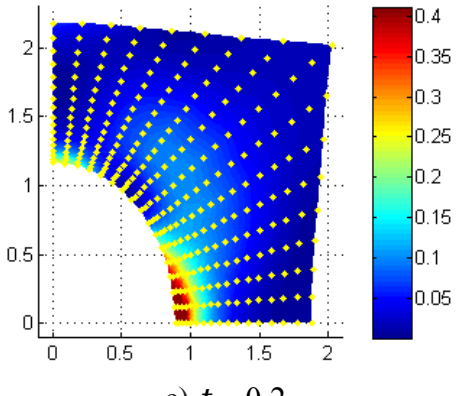

c) $t = 0.2$

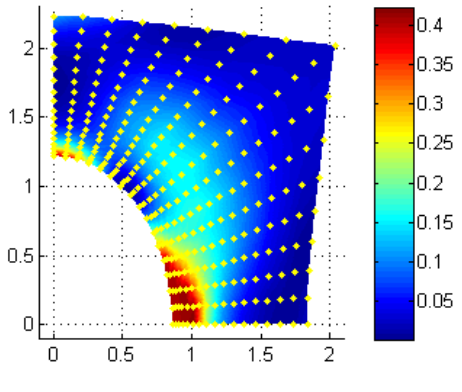

d) $t = 0.25$

Figure 6. Convergence of the elastic strain energy $E = \int_\Omega \boldsymbol{\sigma}_\vartheta : \mathbf{e}_\vartheta d\Omega$ versus the number of degrees of freedom using the FEM-T3 and LC-PIM at $t = 0.2$ for the plate with hole (the solution of the ES-FEM-T3 using a very fine mesh including 28,730 degrees of freedom is used as reference solution)